Journal of the Society of Automotive Engineers Malaysia
Volume 7, Issue 1, pp 32-45, January 2023
e-ISSN 2550-2239

Evaluation of Head and Neck Injuries in Rollover Crashes of Armored Vehicle

M. S. Solah[1,2], **K. S. Tan***[2], W. P. Loh[3], M. Z. Othman[2] and R. M. Sohaimi[2]

[1] Commercial Vehicle Unit, Malaysian Ins. of Road Safety Research (MIROS), 43000 Kajang, Selangor, Malaysia
[2] Dept. of Mechanical Eng., Fac. of Eng., Uni. Pertahanan Nasional Malaysia, 57000 Kuala Lumpur, Malaysia
[3] School of Mechanical Engineering, Universiti Sains Malaysia, 14300 Nibong Tebal, Pulau Pinang, Malaysia

*Corresponding author: keansheng@upnm.edu.my

ORIGINAL ARTICLE *Open Access*

Article History:

Received
15 Sep 2022

Accepted
15 Dec 2022

Available online
1 Jan 2023

ABSTRACT – *Rollover crashes in vehicles often cause deaths. To date, there is no study being conducted on rollover accident injury outcomes involving armored vehicles. This study aimed to examine the driver's response in rollover of SIBMAS 6X6 and to evaluate the severity of head and neck injuries using finite element simulation with Hybrid III 50th percentile male dummy incorporated to represent a driver. The dummy was configured to simulate a typical seated driving posture. The rollover intensity that can produce 180 degrees of rolling with vehicle roof landing was imposed via initial angular velocity that was applied to the whole vehicle. The dummy's head was observed to make three significant impacts on hull interior structures from the initiation of rollover until the roof landed on the ground. Head injury severity was evaluated based on the resultant acceleration of the head center of gravity and 15ms duration Head Injury Criteria (HIC15), whereas neck injury severity was evaluated based on Neck Injury Criteria (Nij). The corresponding highest severity levels recorded in the simulated rollover for these three individual criteria are 531g, 9098, and 2.55. By evaluating these severity values against the respective injury risks and fatality rates as classified in the Abbreviated Injury Scale (AIS), it was clearly indicated that injuries sustained by the driver were mostly fatal.*

KEYWORDS: Abbreviated Injury Scale (AIS), armored vehicles, finite element simulation, rollover crashes, rollover simulations, SIBMAS 6X6

Journal homepage: www.jsaem.my

1. INTRODUCTION

Among the various types of road crashes, rollover crashes occur much less frequently but are disproportionately more dangerous and pose a relatively higher risk of severe injuries and fatality rates than the others. For example, of all motor vehicle crashes in 2020 in the US, only about 2% involved a rollover but it accounted for approximately 30% of all deaths (NHTSA, 2022). In Australia, about 19% of fatal crashes were due to rollover (Rechnitzer & Lane, 1994), while in Europe it is around 10-20% depending on the country (Ferguson, 2007). Compared to typical planar collisions, serious and fatal injuries to the head, neck, and spine are more common in rollover crashes (Yoganandan et al., 1989). For example, the head, brain injury, and hemorrhage accounted for most major injuries, with the remaining attributed to fractures of the skull (Mattos et al., 2013), whereas most of the major injuries for the spine were fractures (Bambach et al., 2013).

The seriousness of deadly rollover incidents also occurred for military armored vehicles. On 6th July 2014, at kilometer 232.6 on the Malaysia North-South Expressways, an army sergeant and a corporal died while two other army personnel suffered injuries when the armored vehicle SIBMAS 6X6 they were in skidded and rammed onto the road divider before it overturned (Astro Awani, 2014). On the other hand, a report from the United States Government Accountability Office (2021) found that 123 soldiers and marines died in 3,753 non-combat tactical vehicle incidents between 2010 and 2019. The report found that despite being responsible for one-quarter of the accidents, rollover crashes accounted for 63% of the deaths reviewed in the study and were the deadliest accidents.

Two apparently contrasting theories of injury causation exist in rollover crashes, viz. diving (Moffat, 1975) and roof intrusion (Friedman & Nash, 2001). The diving theory introduced a concept of torso augmentation, which suggested that head, neck, and spinal injuries result from inertial loading of the torso during a roof-to-ground impact. On the contrary, intrusion theory hypothesized that head and neck injuries in rollover crashes are due to the reduction of headroom associated with roof deformation in combination with the occupant moving toward the ground when the vehicle is inverted. Nevertheless, Hu et al. (2010) propounded that diving is the major injury mechanism in rollovers, and roof stiffness, but not roof crush, which affects the head and neck injury risks for far-side occupants during the diving type of impacts. Obviously, the roof crush theory is only applicable to regular vehicles with deformable body structures. For armored vehicles constructed of an all-around stiff interior, it is expected that the diving/falling type coupled with the stiff roof would be the predominant injury causation.

In view of the high fatality rate involved in rollover incidents and the existence of research gaps that mainly attributed to design characteristics of armored vehicles, particularly in terms of compartment layout and hull rigidity which are totally different from regular passenger cars, sports-utility vehicles, trucks, etc., an effort was thus initiated to research into the relevant injury mechanisms that might be unique to armored vehicles. Specifically, the purpose of the present study was to investigate the driver's behavior and head impacts and to evaluate the severity of head and neck injuries in an under-turn rollover crash by finite element simulation approach. It is in expectation that the findings from the study will provide essential knowledge and useful input which are crucial for designing effective precautions and countermeasures to minimize the related casualties and thus save military personnel's lives in case of such accidents.

2. MODELLING AND SIMULATIONS OF ROLLOVER

2.1 Finite Element Model of Armored Vehicle

The reference armored vehicle used in the present study to simulate rollover crashes is the SIBMAS 6X6 AFSV-90, which measures 7.32m in length, 2.5m in width, 2.24m in height to hull top, and 2.77m to turret top. The wheelbase measured 2.8m for the mid-row wheels and 4.2m for the rear ones. More detailed specifications and key features are available in Foss (2000). As depicted in Figure 1, the SIBMAS hull is constructed of an all-welded steel structure long box-shaped with a horizontal roofline, and inward slope at the front and rear. The driver seat is located at the front, in a space symmetrically between the two protrusions of the hull structure that make allowances for the front wheels. The driver is provided with a single hatch cover and three large windows. On the right side of the vehicle, the troop compartment extends from the right door to the right rear end of the hull where a large door is located for disembarkment, whereas a smaller troop compartment is available on the left side and to the rear of the left door. The engine compartment is in the left rear hull, and the corresponding roof portion can be opened to allow for access to the engine. The turret of a 90-mm gun is located near the hull front, immediately behind the driving compartment, and is provided with three large rectangular hatches. The combat weight of SIBMAS varies between 14.5 to 18.5 tons depending on the role. The AFSV-90 variant can accommodate three (commander, gunner, and driver) plus nine passengers, while as an armored personnel carrier, it can carry a crew of up to sixteen people.

The finite element (FE) model of the SIBMAS was created based on the CAD model created using photogrammetric techniques, which was carried out by the co-author's team in the earlier research. The meshed FE model of partially opened SIBMAS in Figure 2 shows the general layout of the vehicle interior. The SIBMAS body is generally made from high-strength steel of which deformations are negligible during the rollover and thus the detailed material input data is not crucial as it can be modeled as an assemblage of rigid parts. In LS-DYNA, all the individual parts were rigidly connected to each other using the keyword CONSTRAINED_RIGID_BODIES, with the hull being set as the master part.

Most often, relatively coarse meshes are used for rigid parts as deformations can be neglected. However, when modeling contact interfaces between parts, overly coarse meshes may result in contact instability especially when the stiffness of interacting parts is significantly different from each other. Besides, element size does affect the distribution of contact forces. A general guideline is that spacing on the contact surface of a rigid body should be no coarser than the mesh of any deformable part that encounters the rigid body (DYNAmore GmbH, n. d.). In the current simulation, the dummy's various soft parts will come into impact with various rigid hull interiors. Moreover, the focus will be on the dynamics

of the head and neck, which dictates that proper distributions of contact forces during impacts are crucial. Thus, to fulfill the requirements, relatively fine elements, which on average are two to three times finer than those of dummy parts, were used to mesh the whole hull structures. Since there are no stress or strain computations involved for rigid bodies, the effect on CPU requirements is negligible and therefore it is often not encouraged to economize meshing of rigid bodies.

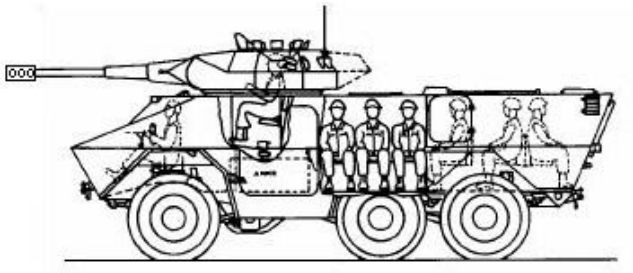

FIGURE 1: Schematic diagram showing seating configurations of SIBMAS (Surlémoant, 1981)

FIGURE 2: Created finite element model of SIBMAS AFSV

The measurement of inertial properties of the SIBMAS without the engine, gearbox, turret, and cannon assembled was carried out experimentally using a crane as reported by Suhaimi et al., 2019. The mass was about 12.4 tons, with the location of the center of gravity (CG) estimated at 2.404m along the *x*-axis with reference to the front axle, and 1.968 m along the *z*-axis with the ground as the datum. The mass moment of inertia was also measured, which were 9.183×10^5 and 1.089×10^6, respectively about the *x*- and *y*-axis, with reference to a pivot point where the vehicle was suspended from the boom of a crane. The corresponding values of mass moment of inertia with reference to its own CG, namely centroidal moment of inertia, can be obtained by applying the Parallel-axis theorem:

$$I_o = I - md^2 \qquad (1)$$

where I_o is the centroidal mass moment of inertia; I is the mass moment of inertia about the targeted axis; and d is the perpendicular distance between the CG and the targeted axis. Resetting these values to be based on CG facilitates the tuning of the inertial properties of the SIBMAS model so that its dynamics would be reasonably comparable to the physical one. The mass moment of inertia of yaw motion, i.e., about the *z*-axis, was not tuned as its effect is not important in roll motion.

The total mass of the created SIBMAS model with the engine, gearbox, turret, and cannon incorporated was 16.78 tons, and the inertial properties are summarised in Table 1.

TABLE 1: Inertial properties of SIBMAS

Inertial Properties	*x*-axis	*y*-axis	*z*-axis
Location of CG as measured from the front axle (m)	2.392 (from front axle)	0.023 (from mid-plane of the vehicle)	0.859 (from ground)
Centroidal mass moment of inertia (kg-m^2)	1.560×10^4	7.059×10^4	7.0384×10^4

2.2 Occupants Setting

A range of crash test dummies are available to represent the distinctive sizes and forms of humans. Considering that the present study is of an exploratory nature primarily focusing on the driver's overall behavior and the impact-contact points with the vehicle interior during a rollover event, a more efficient dummy model, i.e., LSTC Hybrid III Fast Dummy, of 50th percentile male, was employed in current simulations to represent the driver. The dummy model consists of 119 parts, 2,566 deformable elements, 1,712 rigid elements, and 7,074 nodes. Detailed specifications, calibration data, and pre- and post-processing procedures of this model for the purpose of quantitative analysis are documented in Guha et al. (2011).

The position of the dummy was configured to simulate a driver posture, as shown in Figure 2, where it was adjusted to sit on the driver seat, with the buttocks fine-tuned to merely touching the seat surface. The initial seat deformation due to the sinking of the dummy into the seat under gravity was neglected since the chair is made of hard plastic without a cushion. The upper and lower legs were adjusted such that the heels of the shoes were just resting on the cabin floor. The palms were merely touching the steering wheel.

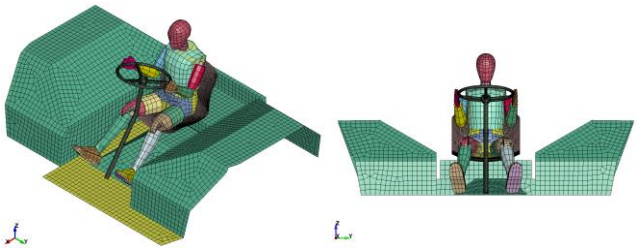

FIGURE 3: Configuration of the dummy on the driver's seat

2.3 Setup of Contact Interfaces

The dummy itself as provided by LSTC already incorporated essential internal contact interfaces among the various dummy parts needed for frontal crash test simulations such that users need to define only the required contact interfaces between the dummy's parts and external structures. However, in trial runs of rollover simulations for the current study, upper legs were observed to invariably penetrate through the pelvic-lower abdominal regions to a significant extent as they rotated upwards, due to the motion of feet that were pushed upwards by the cabin floor when the vehicle started to roll. The action of the upper legs tended to compress the pelvic-lower abdominal regions if the contact exists and thus must be defined. Besides, the "contact-impact" between the various parts of the dummy and the hull interior structures, and between the hull exteriors and the ground, were also added accordingly. These additional contact interfaces were defined by CONTACT_SURFACE_TO_SURFACE and were segment-based type (SOFT = 2).

2.4 Rollover Conditions

To simulate a rollover, an initial angular velocity was imposed on the whole vehicle, with the rotational axis defined to be along the *x*-axis and located at the mid-point of the bottom left tire, i.e., the mid-point of the tire contact patch, such that the vehicle rolled towards the left side of the driver. The minimum lateral velocity required for rollover to happen, v_{min}, can be estimated from the following equation (McHenry & McHenry, 2008):

$$v_{min} = \sqrt{2g(l - z_G)(r^2 + l^2)/{z_G}^2} \qquad (2)$$

whereas the corresponding angular velocity in roll measured in rad per second is given as:

$$\omega = v_{min} z_G/(r^2 + l^2) \qquad (3)$$

where v_{min} is the lateral velocity of the vehicle at the time of initial contact with the trip point; g is the standard gravitational acceleration; z_G is the height of CG from the ground; l is the moment arm of the CG of the vehicle about the trip point; I is the mass moment of inertia of the vehicle about the trip point. On the other hand, the minimum angular velocity in rad per second for lateral rollover beyond 90° rolling can be estimated from the following formula (McHenry & McHenry, 2008):

$$\omega_\theta = \theta\sqrt{g/2[\theta y_G - (z_R - z_G)]} \qquad (4)$$

$$v_\theta = s/t - z_G\omega + (r^2 + {z_G}^2 + {y_G}^2/z_A)\omega \qquad (5)$$

where θ is the roll angle at landing; ω_θ is the angular velocity to attain the θ; v_θ is the lateral velocity to attain the θ; y_G is the lateral distance from the CG of the vehicle to the trip point; z_R is CG elevation at landing.

In order for the dummy to experience some significant extent of diving/falling in a rollover, an initial angular velocity that produced at least 180° at landing was applied, of which the final magnitude was set as 1.9765 rad/s. The initial angular velocity was imposed by INITIAL_VELOCITY_GENERATION.

As it would be impractical to simulate the rollover event until the vehicle came to a complete stop, the simulation duration was thus set to 2.5 s such that less than 5% (3.7% specifically) of the kinetic energy left in the system.

2.5 Severity of Injuries

The severity of head injury can be assessed using two common criteria: the resultant peak acceleration measured at the center of gravity of the head, and the Head Injury Criterion (HIC) score. HIC is a measure of the likelihood of injury arising from an impact, defined by Kleinberger et al. (1998) as:

$$HIC = max\left\{(t_2 - t_1)\cdot\left[\frac{1}{t_2 - t_1}\int_{t_1}^{t_2} a(t)dt\right]^{2.5}\right\} \qquad (6)$$

where t_1 and t_2 are the initial and final times selected to maximize HIC value, with the acceleration measured in standard gravitational acceleration, gs. The time duration from t_1 to t_2 is usually 15ms (HIC15) and is limited to a maximum value of 36ms (HIC36). The HIC15 is more restrictive as it is associated with a higher risk level than the HIC36 for the same HIC score. Moreover, it has been reported by Prasad and Mertz (1985) that the longest HIC duration with either skull fracture or brain damage is 13.7ms, and the duration of the effective part of the impact must be less than 15ms to produce skull fracture or concussion (Hodgson & Thomas, 1972). Therefore, only the HIC15 will be examined in the present study.

HIC scores are correlated with the probability of different severities of head injury that are classified in the Abbreviated Injury Scale (AIS) (AAAM, 2015). The relationship between the HIC and the probability of injury was presented as a group of sigmoidal curves, developed by Prasad and Mertz (1985). These curves can also be described using the following exponential model, with the coefficients corresponding to each of AIS levels as summarized in Table 2:

$$p(\text{AIS}) = 1 - \exp(-a\cdot\text{HIC}^b) \qquad (7)$$

TABLE 2: Coefficient values of the exponential model of equation (6)

AIS Scale	*a*	*b*
Minor (AIS 1)	8.79×10^{-06}	1.94
Moderate (AIS 2)	4.18×10^{-07}	2.24
Serious (AIS 3)	9.00×10^{-09}	2.64
Severe (AIS 4)	2.34×10^{-09}	2.69
Critical (AIS 5)	2.23×10^{-19}	5.66
Usually fatal (AIS 6)	4.76×10^{-31}	9.03

In addition, the probability of skull fracture (AIS≥3) can also be computed (Jin et al., 2020):

$$p(\text{skull fracture}) = N\{[\ln(\text{HIC}) - \mu]/\sigma\} \qquad (8)$$

where μ and σ are the cumulative normal distribution parameters of which $\mu = 7.45231$ and $\sigma = 0.73998$.

For neck injury, one of the common criteria used to evaluate severity is Neck Injury Criteria, N_{ij}, which accounts for the combination of axial loads and bending moments in the upper neck. It is defined as the sum of normalized loads and moments (Kleinberger et al., 1998):

$$N_{ij} = (F_z/F_{int}) + (M_y/M_{int}) \qquad (9)$$

where F_Z is the axial load, M_Y is the flexion/extension bending moment, and F_{int} and M_{int} are the critical intercept values of the load and moment used for normalization, respectively. The intercept values depend on the tested dummy and those for Hybrid III midsize adult males are given in Table 3 (Eppinger et al., 2000). The subscripts ij represent indices for the four different injury mechanisms: tension-extension (N_{TE}), tension-flexion (N_{TF}), compression-extension (N_{CE}), and compression-flexion (N_{CF}).

TABLE 3: Critical intercept values for N_{ij}

N_{ij} Intercept Values			
Tension (N)	**Compression (N)**	**Flexion (Nm)**	**Extension (Nm)**
6806	-6160	310	-135

Complete injury risk curves for AIS 2, 3, 4, and 5 neck injuries have been developed as a function of the calculated N_{ij} value (Eppinger et al., 1999), given as:

$$p(\text{AIS}\geq 2) = 1/[1+ \exp(2.054 - 1.195N_{ij})] \qquad (10)$$

$$p(\text{AIS}\geq 3) = 1/[1+ \exp(3.227 - 1.969N_{ij})] \qquad (11)$$

$$p(\text{AIS}\geq 4) = 1/[1+ \exp(2.693 - 1.195N_{ij})] \qquad (12)$$

$$p(\text{AIS}\geq 5) = 1/[1+ \exp(3.817 - 1.195N_{ij})] \qquad (13)$$

In addition to classifying the injury severity in a six-division ordinal scale running from minor, moderate, serious, severe, critical, to untreatable (usually fatal), each of the AIS scales is indeed associated with risks of threat to life, or rate of fatality, as summarised in Table 4 (Hayes et al., 2007), rather than a comprehensive evaluation of severity of injuries. A nearly perfect nonlinear correlation, i.e., with coefficient determination (R^2) of 0.9934, between AIS severity and survival (as well as mortality) was reported in AIS 2005 (AAAM, 2016).

TABLE 4: AIS levels and the corresponding fatality rates

Severity scale	Injury severity	Fatality rate
1	Minor	0.0
2	Moderate	0.1-0.4
3	Serious	0.8-2.1
4	Severe	7.9-10.6
5	Critical	53.1-58.4
6	Maximum (untreatable)	-

3. RESULTS

3.1 Overall Behavior of Dummy

The overall behavior of the dummy driver during the simulated rollover, from the initiation of a rollover, until the vehicle rolled 180º with the roof hit the ground, is illustrated by a series of sequential images at an interval of 0.2 seconds in Figure 4 (note that the frontal hull portion is removed for proper viewing). Dummy parts that initially have direct contact with vehicle structures are the buttocks and the shoe heels. As the vehicle starts to roll, dynamic forces will be exerted on these two contacting areas immediately, which then transmitted to other body parts. The dummy was seen ejected from the seat towards upper right side as soon as the rolling started. The left leg movement was interfered with by the steering stem as it hit the stem whereas the right leg was thrown upwards with the forces transmitted from floor, and eventually compressed the pelvic-lower abdominal region. This compression only lasted for a very short time of less than 0.1s.

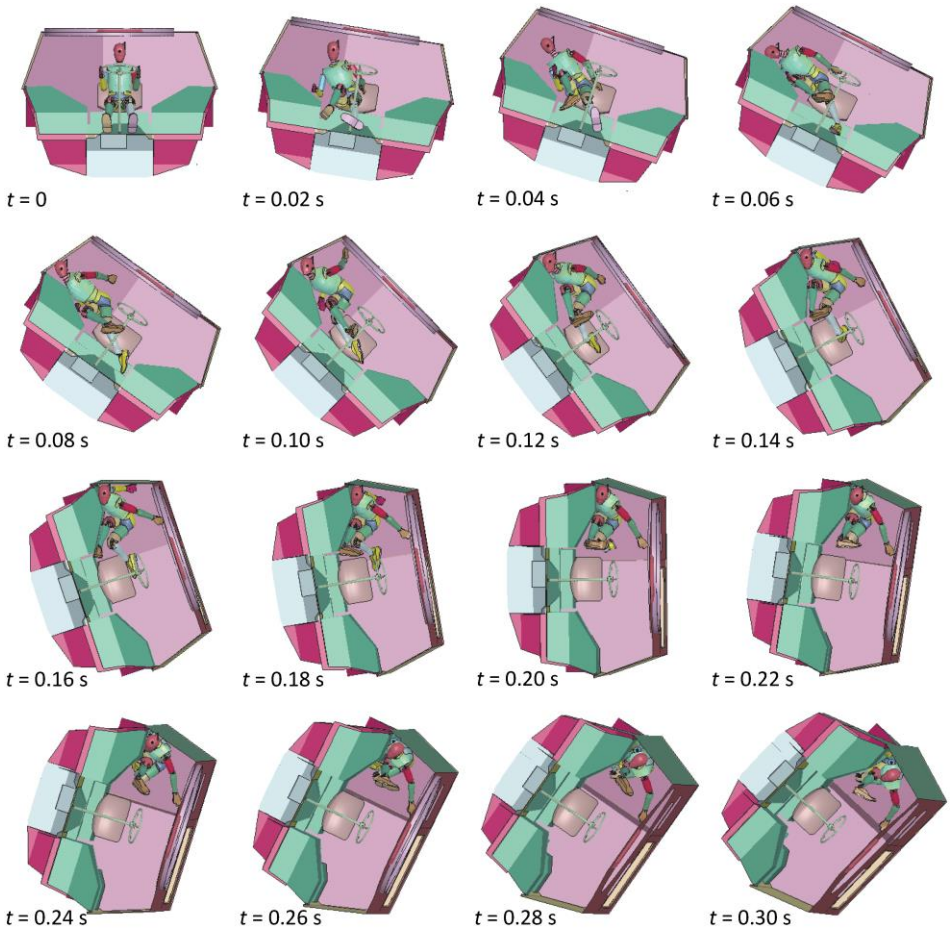

FIGURE 4: Driver's overall behaviour in rollover for initial angular velocity of 1.98 rads^{-1}

The first impact to the head occurred at the upper right portion as it struck the protruding flat surface of the upper-right frontal hull (the location comparable to the right window of a passenger car) at about 0.22 s (Figure 5). The shortening of the neck was observed from 0.215 s (initial contact) to 0.23 s (started to disengage from contact).

As the vehicle continued to roll, the contact-impact forces on the dummy's right body parts produced negative moments (clockwise as view) with the contact point between the right leg and the steering stem forming the pivot. It was seen that from about 1.10 s, the dummy rotated and fell towards the roof and led to the second impact of the head on the hatch cover at about 1.22 s (Figure 6). This second impact was so severe that after the impact, the head rebounced from the structure and moved forward with the neck flexed until the chin impact the upper chest, then followed again by neck extension, bringing the head rearward and consequently caused third impact to the head at about 1.29 s (Figure 6).

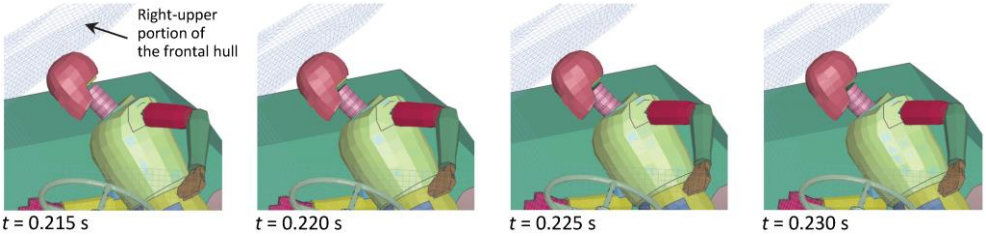

FIGURE 5: First impact to the driver's head

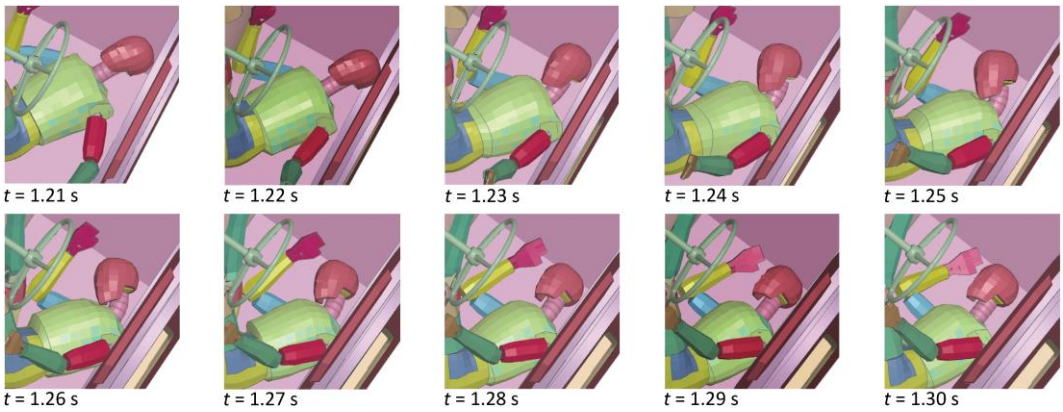

FIGURE 6: Time history of flexion/extension bending moment of the upper neck in rollover

3.2 Head and Neck Responses

Time histories of the head and upper neck dynamic responses are presented in Figures 7 to 14. The three key instants, i.e., 0.22, 1.22, and 1.29 s, at which the head impacts occurred are signified by the corresponding significant spikes in the time history curves of *x*-, *y*-, *z*-components, and resultant accelerations of the head, respectively shown in Figures 7 and 8. The corresponding peak magnitudes of the head resultant acceleration in Figure 7 are 139*g*, 531*g*, and 144*g*, respectively. While the resultant head acceleration is useful in providing the ultimate magnitude sustained by the head, it lacks information about head motions in specific directions, which are useful to relate head kinematics to neck responses. For example, at 1.22s, the significant acceleration along the *x*- and *y*-axis is followed by the significant shear forces in the neck along the corresponding directions (Figure 9). By comparing the neck forces of Figures 9 and 10(a), it is clear that the load was highly dominated by compression especially during the first impact, which was about 25 times higher than shear forces, whereas about six times and three times higher during the second and the third impacts, respectively. In Figure 10(b), the increasing negative moment at about 0.2s shows that the neck experienced some extension (negative moment) in the first head impact, while the transition of the increasing positive moment to the negative one at in the range of 1.2 to 1.3s indicates the neck flexion followed by an immediate extension in the second-third head impacts, as described previously.

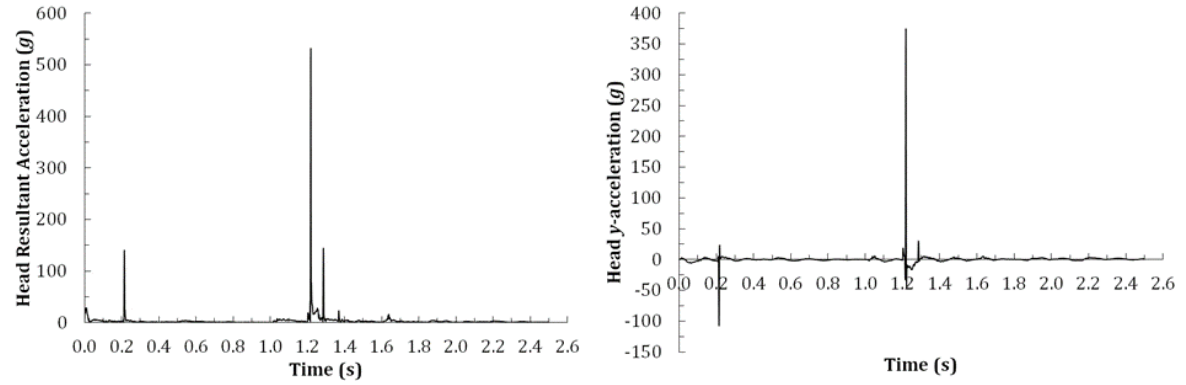

(a) (b)

FIGURE 7: (a) Time history of head resultant acceleration in rollover; (b) Time history of x-acceleration of head in rollover

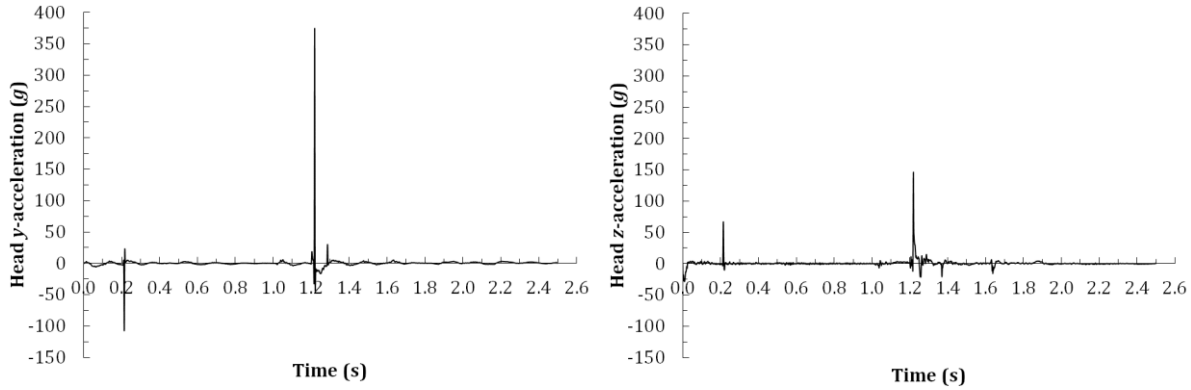

(a) (b)

FIGURE 8: (a) Time history of y-acceleration of head in rollover; (b) Time history of z-acceleration of head in rollover

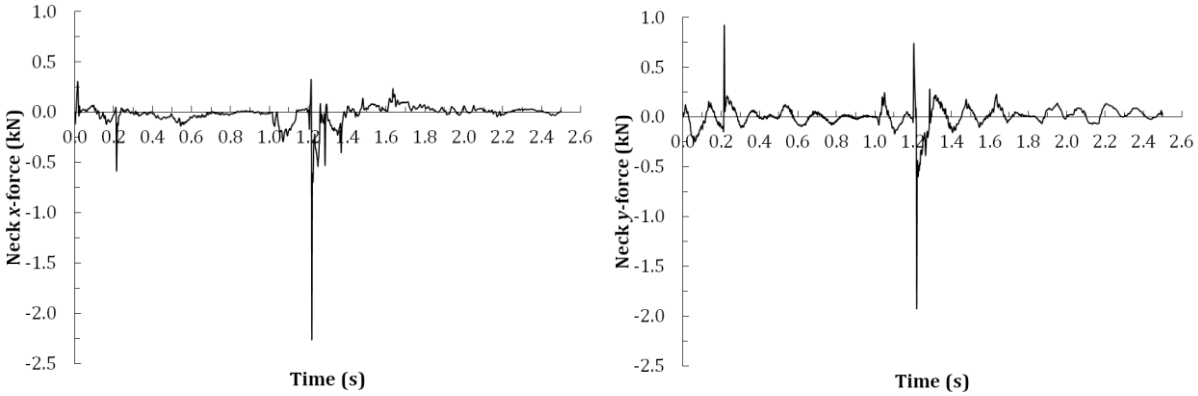

(a) (b)

FIGURE 9: (a) Time history of the x-shear load of the upper neck in rollover; (b) Time history of the y-shear load of the upper neck in rollover

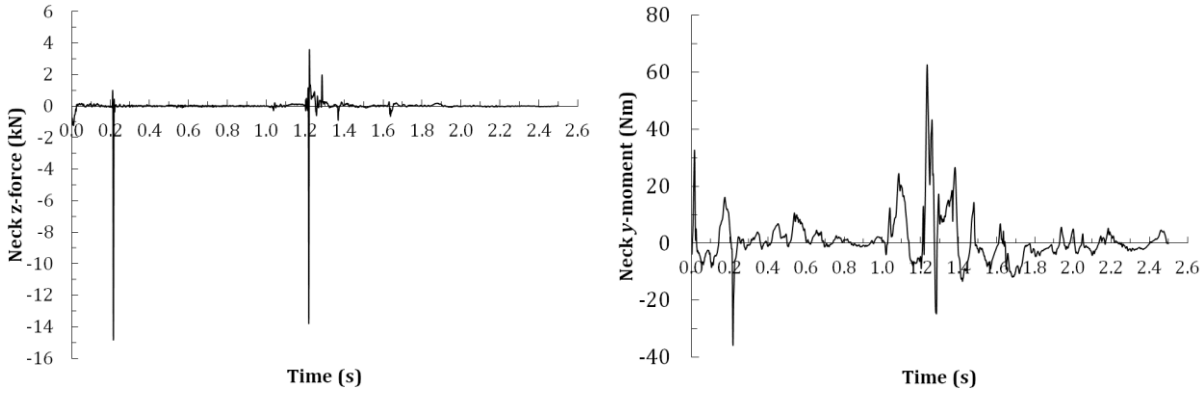

(a) (b)

FIGURE 10: (a) Time history of the axial load of the upper neck in rollover; (b) Time history of extension/flexion bending moment of the upper neck in rollover

3.3 Evaluation of Severity of Injuries

The HIC15 scores in the simulated rollover were found to follow the magnitude order of the head resultant acceleration. The computed highest HIC15 score was 9,098, which corresponds to the second impact that produced the highest peak resultant acceleration, followed by 3,456 and 2,086 of the third and first impacts, respectively.

To assess the severity of neck injury by N_{ij}, the z-force and y-moment curves were first normalized against the respective intercept critical values to yield the individual normalized curves. These two curves were then superposed to obtain the curve of continuous maxima which indicate the N_{ij} at every instant throughout the rollover (Figure 11). The N_{ij} values following the three crucial head impact incidents are summarized in Table 5, along with the dominant loading components. Though the second impact produced the most severe head impact, it did not yield the highest N_{ij} score. The neck injury mode that resulted in the highest N_{ij} values corresponded to compression-extension in the first and second impacts, and tensile-extension in the third impact.

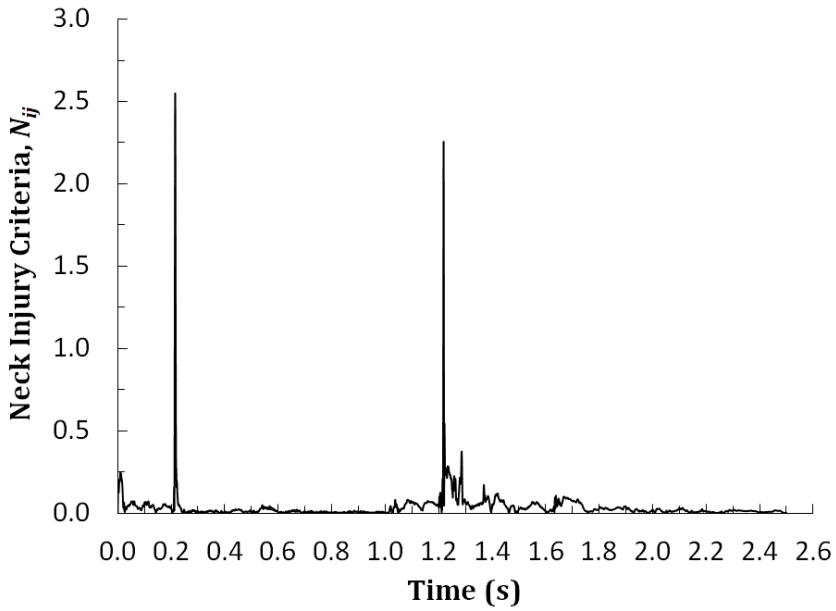

FIGURE 11: Maxima of N_{ij} in rollover

TABLE 5: Neck injury modes and the maximum N_{ij} values following the three head impacts

Impact incident	*z*-force (kN)	*y*-moment (Nm)	N_{ij}
First impact	-14.8	-19.5	2.55
Second impact	-13.8	-2.7	2.26
Third impact	1.8	-14.6	0.38

4. DISCUSSION

The severity of both the head and neck injuries experienced by the dummy in the simulated rollover was significantly higher compared to the corresponding injury assessment reference values (IARVs) for the head and neck. The IARVs are the limits of severity a dummy can sustain for less than a 5% chance of the injury occurring. The limit for HIC15 is 700 for the midsize adult male, which corresponds to a 5% risk of skull fracture and to a 5% risk of AIS≥4 brain injury (Mertz et al., 2003). On the other hand, the IARV based on peak resultant acceleration is 180*g*, which corresponds to a 5% risk of skull fracture (Mertz et al.,1997). Nevertheless, in cases involving serious crashes in which injuries are mostly serious, severe, or even critical, the IARVs are not so useful in assessing severity since the values would mostly be exceeded and the focus then often on chances of survivability, such as the threat to life ranking based on AIS scale (Table 4).

The injury risks associated with HIC15 scores for the three head impacts in the rollover, computed based on Equation (5), are summarised in Table 5. The current rollover condition resulted in the HIC15 scores of 9098 (second impact) and 3456 (first impact) which are extremely high such that even the probability of AIS 6 is 100%, i.e., the definite fatal head injuries. For the peak resultant acceleration, the value at about 410*g* would cause a 99.9% chance of skull fracture (Mertz et al., 1996). In the current simulated rollover outcomes with the peak value of 531*g*, the skull fracture was thus for sure occurred.

TABLE 6: Injury risk associated with head injury based on HIC15 scores

HIC15	*p*(AIS≥2)	*p*(AIS≥3)	*p*(AIS≥4)	*p*(AIS≥5)	*p*(AIS 6)
9098	1	1	1	1	1
3456	1	1	1	1	1
2086	1	0.99	0.86	0.75	0.36

The first impact was clearly predominated by axial loading that exerted on the vertex of the head, which would result in basilar skull fractures without concomitant vault fractures and would also involve fracturing of the occipital condyles without concomitant brain injury (Bambach et al., 2014). Brain injury is always a primary concern in any head impact. Skull fractures with severe brain damage tend to occur at AIS≥4 (Benetton et al., 2017). Clearly, the dummy in the simulated rollover condition was undoubtedly not survivable with critical brain damage, as indicated by the 100% AIS 6 injury level in Table 6.

The limit of IARV based on N_{ij} is 1, which typically represents a 22% risk of an AIS 3 injury. The injury risks associated with N_{ij} are summarized in Table 6. The combination of the bending moment of the neck and the axial compression force, i.e., compression-flexion as in the first and second impacts, can cause wedge fracture of the anterior vertebral body (McElhaney & Myers, 1993). At a sufficiently high force, a burst fracture or bilateral facet dislocation could occur, which results in instability and may disrupt, consequently causing injury to the spinal cord of which the extent of the injury depends on the penetration of the vertebral body or its fragments into the spinal canal. In the current simulation, the resulting N_{ij} score of 2.52 represents a 31% probability of AIS 5+ neck injuries, which usually include complete cord syndrome with quadriplegia or paraplegia. With the associated average fatality rate of 55.75% (Table 7), the current simulated rollover condition thus accounted for about 17% of the risk of fatality, based on neck injuries.

In the current study, it was noted that in head impact incidents the highest HIC or head resultant acceleration does not necessarily yield the highest N_{ij}. This is because HIC does not account for impact direction that will determine the effective loading mode on the neck, such as axial or shear load, lateral bending or flexion-extension, as the impact forces transmitted to the neck and as the head moves

relative to the neck. For example, though during the second impact, the magnitude of the head resultant was much higher, as the impact was mainly towards the back of the head, it caused predominantly shear load to the neck, which was not taken into consideration in the N_{ij} calculation.

TABLE 7: Injury risks associated with neck injury in terms of N_{ij} scores

N_{ij}	p(AIS≥2)	p(AIS≥3)	p(AIS≥4)	p(AIS≥5)
2.52	0.721	0.849	0.577	0.308
2.26	0.655	0.771	0.501	0.246
0.38	0.167	0.077	0.096	0.033

For the SIBMAS with a rigid hull, diving/falling would be the sole injury causation in a rollover as opposed to regular cars, of which cervical spine injuries could be further exacerbated by roof intrusion (Bambach et al., 2014) besides inverted impact with roof structure. However, the high stiffness bare roof without padding in the SIBMAS could increase the severity of head injury. Improper padding of roof structures and framing in regular cars has been found to result in severe head injuries, mainly involving scalp lacerations, fractures of the skull, and brain injury (Rechnitzer & Lane, 1994).

5. CONCLUSION AND RECOMMENDATIONS

The study identifies the severity of head and neck injuries, and the associated injury risks and fatality rates experienced by the 50th percentile male dummy in the rollover of the SIBMAS 6X6 armored vehicle. The study also identifies the potential locations of the head itself and of the vehicle interior where the impacts would most likely occur throughout the rollover. Even at the rollover intensity of two quarter-turns, it could result in absolute fatality. The causes of death mainly due to severe skull fractures, brain injury, and neck fractures. It is recommended that some cushioning elements be placed at potential impact locations in the driver compartment to minimize the severity of injuries. Also, the driver should always apply at least one lap belt to prevent it from ejecting from the seat and subsequently sustaining multiple impacts.

In future studies, initial velocities with combinations of linear and rotational components shall be considered for more realistic simulation conditions. Parametric studies with various rollover intensities shall be conducted to obtain more generalized dummy responses during rollovers. Also, the effects of interactions among passengers, which in turn might affect the contact-impact interactions between the passengers and the vehicle interior, shall also be investigated by incorporating several dummies to represent passengers in the compartment.

ACKNOWLEDGEMENT

This work was supported by the Ministry of Higher Education (MOHE) under Grant No. FRGS/FASA-1-2018/TK01/UPNM/03/3. Part of the work was carried out under LRGS/FASA-1-2018//TK01/UPNM.

REFERENCES

AAAM (2016). Abbreviated Injury Scale 2005 Update 2008. Association for the Advancement of Automotive Medicine (T. Gennarelli, & e. Woodzin, Eds.) Chicago, Illinois.

Astro Awani (2014). Kementerian Pertahanan tubuh lembaga siasat kemalangan kereta perisai. Retrieved from http://www.astroawani.com/berita-malaysia/kementerian-pertahanan-tubuh-lembaga-siasat-kemalangan

Bambach, M. R, Grzebieta, R., McIntosh, A. S., & Mattos G. (2013). Cervical and thoracic spine injury from interactions with vehicle roofs in pure rollover crashes. Accident Analysis & Prevention, 50, 34-43.

Bambach, M. R., Mitchell, R. J., Mattos, G., Grzebieta, R. H. & McIntosh, A. S. (2014). Seriously injured occupants of passenger vehicle rollover crashes in NSW. Journal of the Australasian College of Road Safety, 25(3), 30-40.

Benetton, D., Arosio, B., Anghileri, M., Mongiardini, M., & Mattos, G. (2017). Evaluation of head and brain injury using empirical and analytical predictors in human body model. Paper presented at TRB First International Roadside Safety Conference, California, USA.

DYNAmore GmbH (n.d.). Rigid body contact. Retrieved from https://www.dynasupport.com/tutorial/contact-modeling-in-ls-dyna/rigid-body-contact

Eppinger, R., Sun, E., Bandak, F., Haffner, M., Khaewpong, N., Maltese, M., Kuppa, S., Nguyen, T., Takhounts, E., Tannous, R., Zhang, A., & Saul, R. (1999). Development of improved injury criteria for the assessment of advanced automotive restraint systems - II (NHTSA Doc. 1999-11-01). Washington D.C.: National Highway Traffic Safety Administration.

Eppinger, R., Sun, E., Kuppa, S., & Saul, R. (2000). Supplement: development of improved injury criteria for the assessment of advanced automotive restraint systems - II. Washington D.C.: National Highway Traffic Safety Administration.

Ferguson, S.A. (2007). The effectiveness of Electronic Stability Control in reducing real-world crashes: A literature review. Traffic Injury Prevention, 8, 329-338.

Foss, C. F. (2000). Jane's Tanks and Combat Vehicles Recognition Guide (2nd ed.). HarperCollins.

Friedman, D., & Nash, C. E. (2001). Advanced roof design for rollover protection. Paper presented at the 7th International Technical Conference on the Enhanced Safety of Vehicles. Amsterdam, Netherlands.

Government Accountability Office (2021). Military vehicles – Army and marine corps should take additional actions to mitigate and prevent training accidents. GAO-21-361. Retrieved from https://www.gao.gov/as sets/gao-21-361.pdf

Guha, S., Bhalsod, D., & Krebs, J. (2011). LSTC Hybrid III 5th fast dummy positioning & post-processing documentation. MI: Livermore Software Technology Corporation.

Hayes, W. C., Erickson, M. S., & Power, E. D. (2007). Forensic Injury Biomechanics. Annual Review of Biomedical Engineering, 9(1), 55-86.

Hodgson, V., & Thomas, L. (1972). Effect of long-duration impact on head (SAE Technical Paper 720956). Warrendale: SAE International.

Hu, J., Ma, C., Chou, C. C., & Yang, K. H. (2010). Finite element analysis of occupant head and neck injury mechanism during rollover crashes. International Journal of Vehicle Design, 54(3), 238-261.

Jin, H., Sharma, R., Meng, Y., Untaroiu, A., Doerzaph, Z., Dobrovolny, C. S., & Untaroiu, C. D. (2020). Evaluation of the injury risks of truck occupants involved in a crash as a result of errant truck platoons. SAE International Journal of Transportation Safety, 8(1), 5-18.

Kleinberger, M., Sun, E., Eppinger, R., Kuppa, S., & Saul, R. (1998). Development of improved injury criteria for the assessment of advanced automotive restraint systems (NHTSA Doc. 98-4405-9). Washington D.C.: National Highway Traffic Safety Administration.

Mattos, G., Grzebieta, R., Bambach, M. R., & McIntosh, A. S. (2013). Head injuries to restrained occupants in single-vehicle rollover only crashes. Traffic Injury Prevention, 14(4), 360-368.

McHenry, R. R., & McHenry, B. G. (2008). Accident Reconstruction. McHenry Training Seminar 2008. McHenry Software Inc.

McElhaney, J. H., & Myers, B. S. (1993). Biomechanical aspects of cervical trauma. In: Nahum A.M., Melvin J.W. (Eds). Accidental Injury: Biomechanics and Prevention (pp. 311-361). New York: Springer.

Mertz, H. J., Prasad, P., and Nusholtz, G. (1996). Head injury risk assessment for forehead impacts (SAE Technical Paper 960099). Warrendale: SAE International.

Mertz, H. J., Prasad, P., and Nusholtz, G. (1997). Head injury risk assessment based on 15 ms HIC and peak head acceleration criteria. In AGARD Conference Proceedings 597 (pp 11-1 – 11-9). France: NATO STO.

Mertz, H. J., Irwin, A. L., & Prasad, P. (2003). Biomechanical and scaling bases for frontal and side impact injury assessment reference values. Stapp Car Crash Journal, 47, 155-188.

MHTSA (2022). Traffic Safety Facts Annual Report. National Highway Traffic Safety Administration. Retrieved from https://cdan.nhtsa.gov/SASStoredProcess/guest

Prasad, P., & Mertz, H.J. (1985). The position of the United States delegation to the ISO Working Group 6 on the use of HIC in the automotive environment (SAE Technical Paper 851246). Warrendale: SAE International.

Rechnitzer, L., & Lane, J. (1994). Rollover crash study – Vehicle design and occupant injuries. Report No. 65. Retrieved from https://www.monash.edu /__data/assets/pdf_file/0018/217035/muarc065.pdf

Suhaimi, K., Risby, M. S., Tan, K. S., Syafiq, A., & Hafizi, N. (2019). Heavy military land vehicle mass properties estimation using hoisting and pendulum motion method. Defence Science Journal, 69(6), 550-556.

Surlémoant, R. (1981). SIBMAS – Wheeled armored vehicle. Armor, 90(2), 16-19.

Yoganandan, N., Haffner, M., Maiman, D. J., Nichols, H., Pintar, F. A., Jentzen, J., Weinshel, S. S., Larson, S. J., & Sances Jr., A. (1989). Epidemiology and injury biomechanics of motor vehicle related trauma to the human spine. Journal of Passenger Cars, 98(6), 1790-1809.